Title

Actinide Separation Inspired by Self-Assembled Metal—Polyphenolic Nanocages

Journal

Journal of the American Chemical Society, 142(39)

ISSN

0002-7863

Authors

Mei, Lei

Ren, Peng

Wu, Qun-yan

et al.

Publication Date

2020-09-30

DOI

10.1021/jacs.0c08048

Peer reviewed

Actinide separation inspired by self-assembled metal-polyphenolic nanocages

Lei Mei,[†, §,*] Peng Ren,[†, ‡, §] Qun-yan Wu,[†] Yu-bin Ke,[#] Jun-shan Geng,[†] Kang Liu,[†] Xue-qing Xing,[⊥] Zhi-wei Huang,[†] Kong-qiu Hu,[†] Ya-lan Liu,[†] Li-yong Yuan,[†] Guang Mo,[⊥] Zhong-hua Wu,[⊥] John K Gibson,[&] Zhi-fang Chai,[†, ¶] Wei-qun Shi[†, *]

[†] Laboratory of Nuclear Energy Chemistry, Institute of High Energy Physics, Chinese Academy of Sciences, Beijing 100049, China

[‡] State key Laboratory of Nuclear Resources and Environment, School of Chemistry, School of Nuclear Science and Engineering, East China University of Technology, Nanchang 330013, China.

[⊥] Beijing Synchrotron Radiation Facility, Institute of High Energy Physics, Chinese Academy of Sciences, Beijing 100049, China

[#] Spallation Neutron Source Science Center, Dongguan 523803, China

[¶] Engineering Laboratory of Advanced Energy Materials, Ningbo Institute of Industrial Technology, Chinese Academy of Sciences, Ningbo 315201, China

[&] Chemical Sciences Division, Lawrence Berkeley National Laboratory (LBNL), Berkeley, California 94720, USA

KEYWORDS: actinides; nano-extraction; uranyl-organic nanocage; self-assembly; pyrogallol[4]arene

ABSTRACT: The separation of actinides has a vital place in nuclear fuel reprocessing, recovery of radionuclides and remediation of environmental contamination. Here we propose a new paradigm of nanocluster-based actinide separation, namely nano-extraction, that can achieve efficient sequestration of uranium in an unprecedented form of giant coordination nanocages using a cone-shaped macrocyclic pyrogallol[4]arene as the extractant. The U_{24}-based hexameric pyrogallol[4]arene nanocages with distinctive $[U_2PG_2]$ binuclear units (PG = pyrogallol), that rapidly assembled in situ in monophasic solvent, were identified by single-crystal XRD, MALDI-TOF-MS, NMR, and SAXS/SANS. Comprehensive biphasic extraction studies show that this novel separation strategy has enticing advantages such as fast kinetics, high efficiency, and good selectivity over lanthanides, and thus demonstrate its potential for efficient separation of actinide ions.

As a central component of nuclear fuel processing, actinide separation is crucial for recovery and recycling of key radionuclides.[1-2] Other applications that require efficient radionuclide capture include remediation of environmental contamination,[3] emergency response to nuclear accidents,[4-5] and uranium extraction from seawater.[6-9] Two established approaches to actinide separation are solvent extraction and solid adsorption, with the former dominant due to its adaptability to complex real-world systems and applicability to large-scale operations.[10]

Traditional actinide extraction is achieved through selective complexation of actinide cations from mixtures containing multiple metal ions by exquisitely designed organic extractants.[2, 11-12] Nevertheless, the use of large cluster compounds for actinide separations has been rarely pursued, despite extensive studies of well-defined actinide assemblies that remain intact in solution, including inorganic-organic hybrid polyhedra[13-15] and inorganic nanoclusters bridged by oxide, peroxide, or hydroxide groups.[16-19] In contrast to simple complexes, such assemblies, especially metal-organic coordination assemblies with nanometer-scale dimensions, impose strict requirements on both molecular geometries of the constituent ligands and their coordination preference for targeted metal ions (Figure 1a), an effect termed "multivalent cooperativity".[20-23] Only metal-ligand couples that meet both geometry and coordination criteria are candidates for effective multi-component nano-assembly. Such cooperativity could lead to highly selective formation of exquisite multinuclear assemblies by efficiently excluding undesired ions. Another attribute of this approach is that multivalent interactions can result in remarkable enhancement in stability of the produced supramolecular architectures, which facilitates both extraction and sequestration.

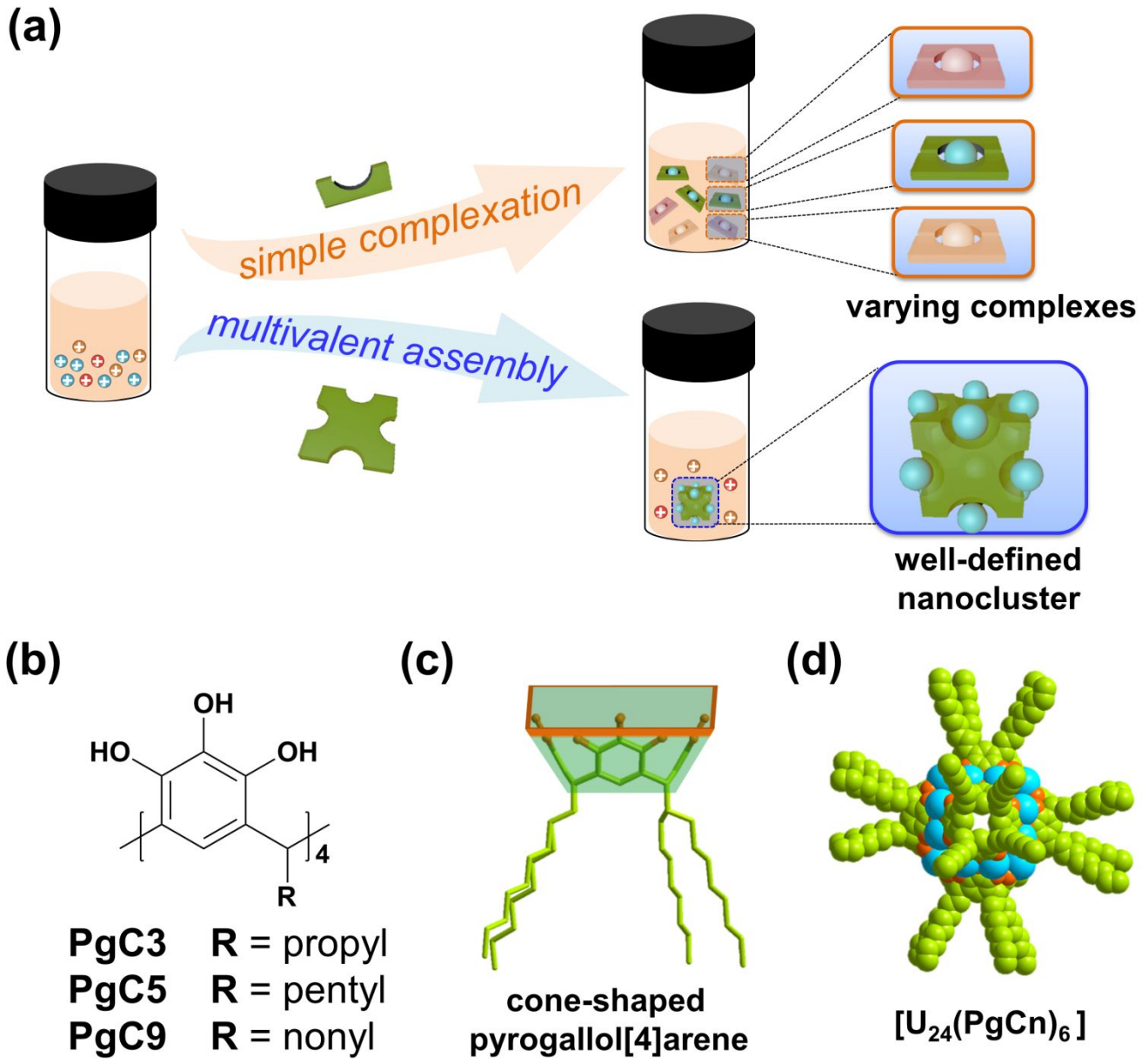

Figure 1. Actinide sequestration based on self-assembled nanoclusters *via* multivalent cooperativity: (a) coordination and capture of actinide ions via simple complexation, or as a well-defined nanocluster; (b) molecular structure of PgCn (n = 3, 5 or 9); (c) model of cone-shaped backbone of PgCn; (d) giant uranyl-polyphenolic coordination cage.

Motivated by characteristics of such cooperativity, a novel strategy for efficient separation of actinides by multivalent assembly of well-defined metal-organic nanoclusters is proposed herein. As a proof of this new concept, we demonstrate sequestration of uranyl ion (UO_2^{2+}) by macrocyclic polyphenolic ligands, *C*-alkylpyrogallol[4]arenes (abbreviated as PgCn, where n is the number of carbon atoms in the alkyl chain, Figure 1b). The cone-shaped PgCn, which is the tetramer of the natural phenolic mimic pyrogallol (PG) with variable length side-chain groups (Figure 1c), has been demonstrated as a versatile precursor for construction of metal-organic nanocapsules.[24-34] Based on coordination assemblies of PgCn (n = 3, 5 or 9) with actinides ions, we have achieved high-performance uranyl capture via uranyl-PgCn nanocages (Figure 1d) assembled *in situ* in monophasic or biphasic solvent systems. This type of extraction as nanoscale species is unprecedented for actinide ions and it leads to a novel paradigm for hybrid nanocluster-based actinide sequestration, which may be considered as "nano-extraction".

Coordination of small-molecule polyphenolic ligand PG with uranyl was considered first. We reported the crystal structure of the resulting complex, U_PG (Table S1), which represent the first crystal structure assessment of uranyl coordination by polyphenol ligands.[35-36] In U_PG, doubly-

deprotonated PG molecules chelate a pair of uranyl ions to form a $[U_2(PG)_2]$ moiety (Figure S1). Density functional theory (DFT) calculations indicate that the residual phenolic proton in U_PG likely occupies a protonated μ_1-OH site, which orients far away from the corresponding μ_1-OH site on the opposing PG ligand (type A in Figure S2 and Table S2). This configuration leads to relatively lower affinity of the protonated μ_1-OH site towards uranium (σ bonding character, Figure S3 and Table S3-S4).

Based on the distinctive coordination of PG towards uranyl, complexation and assembly of pyrogallol[4]arene and uranyl was pursued. Starting with the PgC3 ligand (Figure S4), the UV-vis absorbance spectra of the solution after reaction between a pink solution of PgC3 and uranyl in DMF (Figure S5). It is attributed to strong ligand-to-metal charge transfer (LMCT) from pyrogallol anion to uranyl,[37-38] and thus indicates effective complexation of uranyl in monophasic solvent. The UV-vis spectra of crystal samples resulting from reactions of PgC3 with uranyl similarly exhibit strong LMCT absorbance from 600 nm to 350 nm (Figure S6). Molecular structures were subsequently pursued for the products of reactions between uranyl and PgCn. The crystal structures of U_PgC3 and U_PgC5 show that both have as primary building blocks isolated uranyl-pyrogallol[4]arene coordination cages, $[(UO_2)_{24}(H_2O)_{24}(PgCn)_6]$ (n = 3 or 5; Figure 2a-c and Figure S7), with differences in the side chain length n resulting in different lattice packing modes (Figure S8). Although several pyrogallol[4]arene-based metal-organic nanocapsules (MONCs) have been reported[24-28, 30, 32, 34, 39-40], the $[U_{24}(PgCn)_6]$ motif is the first metal-pyrogallol[4]arene coordination cages based on actinide nodes. Crystals of U_PgC9 suitable for single crystal X-ray diffraction were hard to be obtained (Figure S9), presumably due to the long nonyl side chains hindering close packing of the nanocages. As an alternative, evidences for U_PgC9 with a nanocage structure (Figure S10-S12) as well as the presence of nanocage species upon dissolution (see below) are provided as compared to those for U_PgC3 and U_PgC5. For instance, there is weakening of the hydroxyl vibration modes, and emerging of [O=U=O] stretching modes around 900 cm^{-1} after the transformation of PgC9 to U_PgC9 (Figure S10). U_PgC9, like other two nanocage compounds, shows fluorescence quenching (Figure S11), which is contrast to small complex U_PG and might be closely related to the interference between adjacent groups within the cage. TGA results also demonstrate the similarity of these three nanocage compounds (Figure S12).

Closer consideration of the U_PgCn structures shows that the $[U_{24}(PgCn)_6]$ nanocages are constructed from $[U_2PG_2]$ binuclear nodes like U_PG (Figure 2d). Notably, the $[U_2PG_2]$ motif is quite disparate from trinuclear $[M_3PG_3]$ moiety that is ubiquitous in other metal-seamed hexameric pyrogallol[4]arene nanocapsules.[24-25, 28, 30, 32, 34, 39-40] This difference might reflect the larger effective radius and distinct coordination behavior of the uranyl moiety versus bare transition metals, main group and alkaline earth metals. Different coordination linkages furthermore lead to intriguing characteristics of the topological structures of uranyl-polyphenolic nanocages. Considering vanadium-based hexameric pyrogallol[4]arene compounds for comparison,[28] there is a direct correspondence between the 24 metal atoms that form truncated cubes in $[U_{24}(PgC3)_6]$ and $[V_{24}(PgC3)_6]$ (Figure S13), though the cone-shaped pyrogallol[4]arene ligands that cover the six faces of the cube adopt different orientations. Specifically, four arms of the pyrogallol[4]arene in $[U_{24}(PgC3)_6]$ define four regular sides of a truncated cube (Figure S13b-d), while those in $[V_{24}(PgC3)_6]$ define four inclined sides of an octagonal face (Figure S13f-h). The topological difference between $[V_{24}(PgC3)_6]$ and $[U_{24}(PgC3)_6]$ can be considered as a reorganization of tetratopic cone-shaped pyrogallol[4]arenes through an in-plane rotation accompanied by slight reorganization (Figure S13i).

Crystals of U_PgCn (n = 3, 5 or 9) were dispersed in organic solvents for solution characterization. All three complexes in DMF show wide absorbance in the UV-visible region, with a maximum absorption at ~394 nm (Figure S14). Cyclic voltammetry shows that the uranium centers in all three complexes exhibit the +6 oxidation state characteristic of uranyl (Figure S15). Tyndall scattering phenomenon (Figure S16) is consistent with nanoscale features of $[U_{24}(PgCn)_6]$. Small angle X-ray scattering (SAXS) and neutron scattering (SANS) were employed to probe nanocage aggregation, in lieu of dynamic light scattering that is inapplicable to light-absorbing nano-systems. From the SAXS results, U_PgC3 dispersed in solution can be modeled as a sphere (Figure 2e) with dimensions close to those for the nanocage obtained from crystal data (Figure S17-18). The SANS results further demonstrate the structural integrity of the nanocages dispersed in solution (Figure 2f), and provide information on the side chains, and thus the full extended nanocage radius (Figure S19), due to higher neutron sensitivity to light elements C, H and O. MALDI-TOF mass spectra show broad peaks with m/z values consistent with the theoretical molecular weights (Figure S20), thus providing additional evidence for intact nanocages in solution. Hexameric assembly of PgCn as $[U_{24}(PgCn)_6]$ nanocages in solution is also indicated by aggregation-induced downfield shifts of ^{1}H-NMR peaks assigned to aryl and alkyl groups (Figure S21). In contrast, there is essentially no difference between the chemical shifts for simple PG versus U_PG under these conditions.

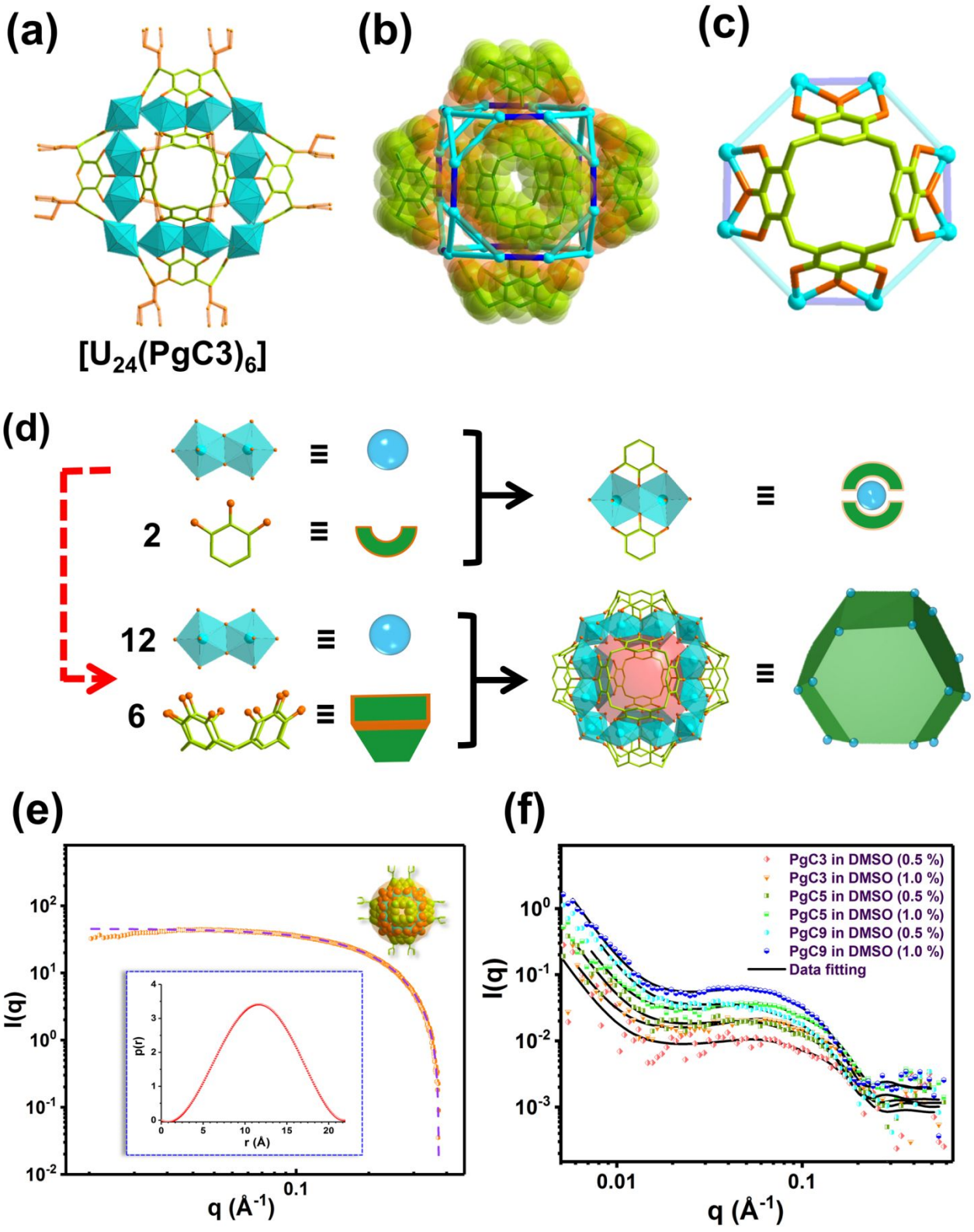

Figure 2. Crystal structure and solution properties of U_PgC3. (a) structural representations of hexameric pyrogallol[4]arene nanocage; (b) a truncated cube formed by all 24 U centers; (c) an octagonal side of the cube with cone-shaped pyrogallol[4]arenes highlighted; (d) construction of U_{24}-based nanocage with the model $[U_2PG_2]$ binuclear motif as the building unit. Turquoise balls or polyhedral are metal nodes; orange balls are oxygen donors; (e) SAXS results for U_PgC3 in DMF, with experimental data as yellow hexagons and the fit using a monodispersed sphere model as black

dashed line. Insert: pair-distance distribution function p(r), suggests a sphere-like model for U_PgC3 (fitting Rg = 8.6 Å corresponds to diameter 22.2 Å); (f) SANS curves for U_PgC3, U_PgC5 and U_PgC9 in solution at two concentrations.

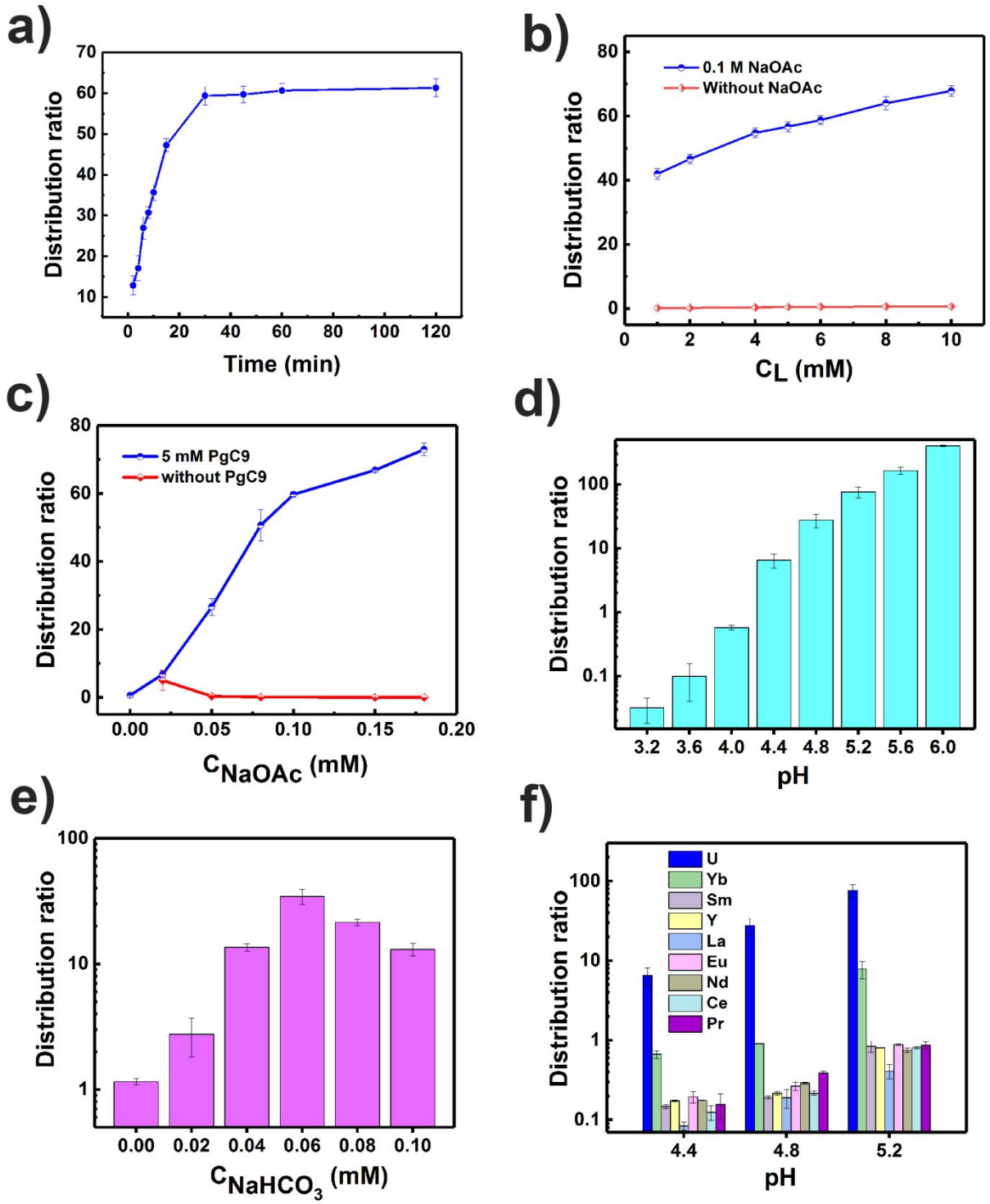

Figure 3. Biphasic nano-extraction of uranium from aqueous phase using PgC9 in water-immiscible DCE or chloroform: (a) extraction kinetics in DCE; (b) effect of concentration of PgC3 extractant on distribution ratio D; (c) effect of concentration of NaOAc on D; (d) effect of aqueous solution pH on D; (e) uranyl extraction in $NaHCO_3$ aqueous solution simulating weakly alkaline seawater; (f) selectivity towards uranyl over lanthanide ions at different pH.

Inspired by uranyl capture in monophasic solution, we pursued this approach for uranyl sequestration in a biphasic system using the PgC9 ligand with long side chains, that shows enhanced solubility in less polar water-immiscible solvents such as 1, 2-dichloroethane (DCE) and chloroform. PgC9 retains coordination activity in these halogenated alkane solvents as it does in DMF (Figure S22). Kinetics in DCE show fast extraction, with equilibrium attained within 30 min (Figure 3a). The distribution ratio (D) increases gradually with the amount of ligand (Figure 3b). Extraction by PgC9 in chloroform is slightly better than in DCE (Figure S23). Adding weak base (NaOAc), or adjusting the solution pH with a buffer (NaOAc-HOAc), significantly affects extraction efficiency (Figure 3c and 3d). More efficient uranyl extraction at lower acidity or higher concentration of NaOAc reflects the necessity to deprotonate the polyphenolic ligand to allow metal ion coordination. Separation in the presence of sodium bicarbonate ($NaHCO_3$) was also demonstrated as comparable to that for the NaOAc system (Figure 3e). Notably, the extraction efficiency towards uranyl is two orders of magnitude higher than for most trivalent lanthanide ions except Yb^{3+} ion with the smallest radius among these lanthanides studied (Figure 3f and Table S5), indicating good selectivity as revealed by moderate separation factors (SF) (Table S6). Back-extraction of uranyl by 1.5 M-2.5 HNO_3 affords 44.7%-40.6% recovery once (Figure S24), can reach over 95% after three times.

Extraction of UO_2^{2+} by PgC9 monitored by UV-vis spectroscopy of the aqueous component reveals a dramatic decrease of the uranyl absorbance (Figure 4). A linear fitting of the distribution ratios to the ligand concentration yields a slope of ~0.21, which is close to the ideal value of 0.25 from the PgC9/U ratio of 6/24 for the model $[U_{24}(PgC9)_6]$ nanocage (Figure S25). The extracted species in the organic component was identified by comparison of the organic phase after extraction with a standard U_PgC9 crystal sample dissolved in the same solvent, using UV-Vis spectroscopy (Figure 4d), mass spectrometry (Figure 4e) and ^1H NMR (Figure S26). The results show that the extracted species is a giant uranyl-containing nanocluster that is at least very similar, possibly identical, to U_PgC9. Compared to a similar biphasic extraction for selectively extraction of pre-synthesized water-soluble uranyl peroxide capsules into organic media by ion exchange,[41] the key merit of the method reported here is in situ multivalent assembly to selectively fabricate the uranyl-polyphenolic clusters to achieve the separation without the necessity of pre-assembly of clusters.

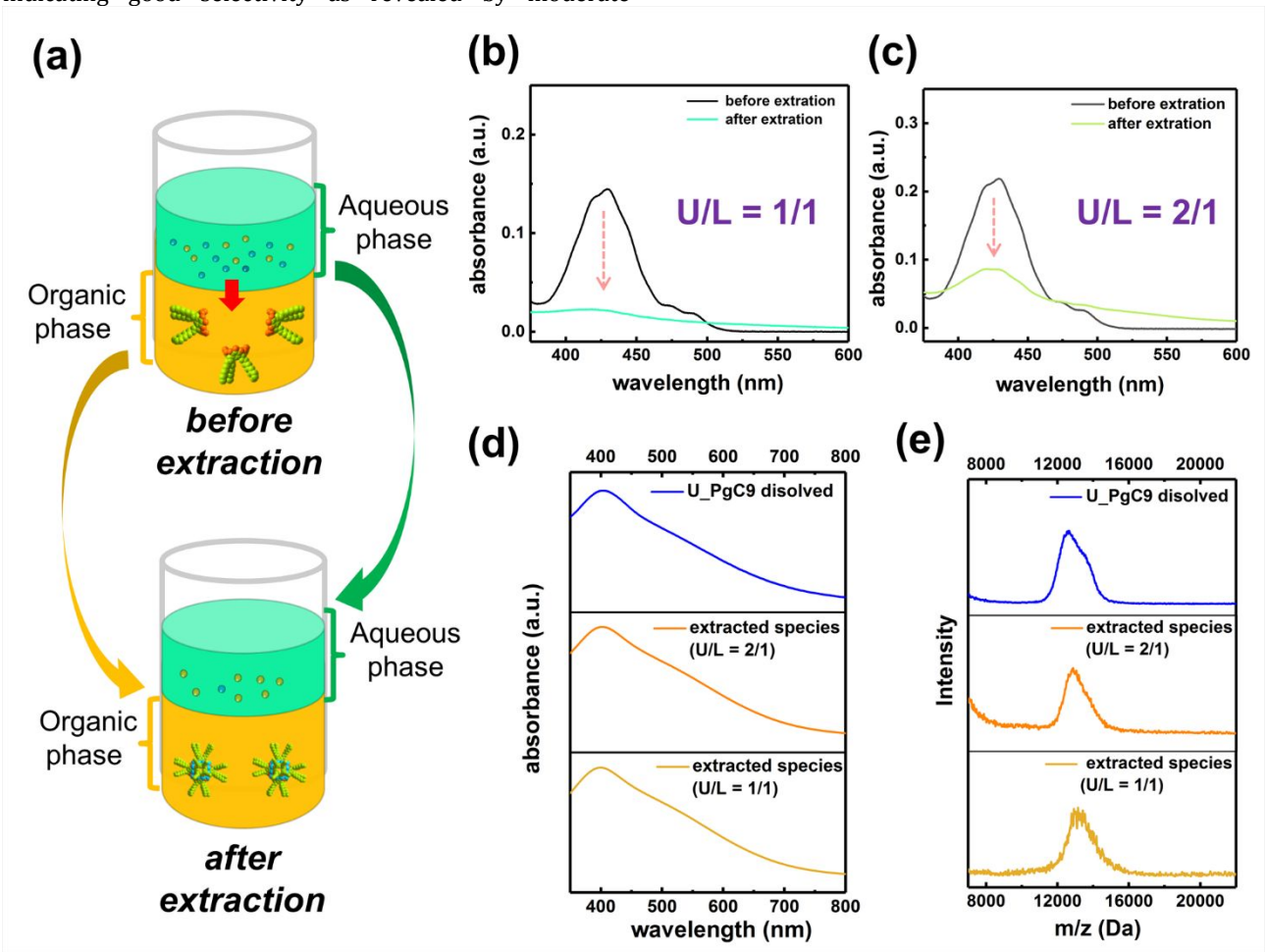

Figure 4. Identification of the extraction product: (a) schematic diagram of the biphasic uranyl extraction process; (b-c) UV-vis spectroscopy of the aqueous phase before and after extraction, for uranyl/extractant (U/L) ratios 1/1 and 2/1, showing

a dramatic decrease of uranyl absorbance upon extraction; (d) UV-vis spectra and (e) MALDI-TOF mass spectra show correspondence between extracted species in the organic layer and U_PgC9 in chloroform.

In summary, uranyl-pyrogallol[4]arene coordination nanocages assembled in situ in solution are identified as new nanocluster-based extraction species for efficient uranium sequestration using monophasic and biphasic solvent systems. Advantages of this extraction strategy include fast kinetics, and good separation efficiency and selectivity. The method furthermore presents a new strategy for extraction of other actinide ions, and a representative paradigm for nanocluster-based actinide separations. Future efforts in this realm should optimize ligand design for improved efficiency and better adaptability, as well as utility in real-world separations such as the separation of U from other actinides such as Np and Pu.

ASSOCIATED CONTENT

Details for synthesis and characterization methods, experimental procedures of uranyl extraction, and computational methods are given in the Supporting Information. The X-ray crystallographic coordinates for reported structures have been deposited in the Cambridge Crystallographic Data Center under accession numbers CCDC: 2014488 (U_PG), 2014489 (PgC3_EtOAc), 2014490 (U_PgC3), and 2014491 (U_PgC5). These data can be obtained free of charge via http://www.ccdc.cam.ac.uk/data_request/cif).

AUTHOR INFORMATION

Corresponding Author

* shiwq@ihep.ac.cn; meil@ihep.ac.cn

Author Contributions

§ These authors contributed equally.

ACKNOWLEDGMENT

We are grateful to Dr. Han-qiu Jiang at Spallation Neutron Source Science Center (Guangdong, China) for the help in small-angle neutron scattering test and data analysis. We also thank Prof. Tai-wei Chu and Dr. Ze-jun Li of Peking University and Prof. Wen Feng and Prof. Li-hua Yuan of Sichuan University for their valuable discussions and suggestions. We thank the support from the National Science Fund for Distinguished Young Scholars (21925603). The National Natural Science Foundation of China (11875057, 21671191 and 21906020) and the Youth Innovation Promotion Association of CAS (2020014) are also acknowledged. The work of J. K. G. was supported by the U.S. Department of Energy, Office of Basic Energy Sciences, Heavy Element Chemistry program at LBNL under Contract No. DE-AC02-05CH11231.

REFERENCES

1. Veliscek-Carolan, J. Separation of actinides from spent nuclear fuel: A review. *J. Hazard. Mater.* **2016,** 318, 266-281.

2. Mathur, J. N.; Murali, M. S.; Nash, K. L. Actinide partitioning - A review. *Solvent Extr. Ion Exch.* **2001,** 19, 357-390.

3. Li, J.; Wang, X. X.; Zhao, G. X.; Chen, C. L.; Chai, Z. F.; Alsaedi, A.; Hayat, T.; Wang, X. K. Metal-organic framework-based materials: superior adsorbents for the capture of toxic and radioactive metal ions. *Chem. Soc. Rev.* **2018,** 47, 2322-2356.

4. Hirose, K. 2011 Fukushima Dai-ichi nuclear power plant accident: summary of regional radioactive deposition monitoring results. *J. Environ. Radioactiv.* **2012,** 111, 13-17.

5. Devell, L.; Tovedal, H.; Bergstrom, U.; Appelgren, A.; Chyssler, J.; Andersson, L. Initial Observations Of Fallout From the Reactor Accident at Chernobyl. *Nature* **1986,** 321, 192-193.

6. Abney, C. W.; Mayes, R. T.; Saito, T.; Dai, S. Materials for the Recovery of Uranium from Seawater. *Chem. Rev.* **2017,** 117, 13935-14013.

7. Kim, J.; Tsouris, C.; Mayes, R. T.; Oyola, Y.; Saito, T.; Janke, C. J.; Dai, S.; Schneider, E.; Sachde, D. Recovery of Uranium from Seawater: A Review of Current Status and Future Research Needs. *Sep. Sci. Technol.* **2013,** 48, 367-387.

8. Liu, C.; Hsu, P. C.; Xie, J.; Zhao, J.; Wu, T.; Wang, H. T.; Liu, W.; Zhang, J. S.; Chu, S.; Cui, Y. A half-wave rectified alternating current electrochemical method for uranium extraction from seawater. *Nat Energy* **2017,** 2, 17007.

9. Parker, B. F.; Zhang, Z.; Rao, L.; Arnold, J. An overview and recent progress in the chemistry of uranium extraction from seawater. *Dalton Trans.* **2018,** 47, 639-644.

10. Keener, M.; Hunt, C.; Carroll, T. G.; Kampel, V.; Dobrovetsky, R.; Hayton, T. W.; Menard, G. Redox-switchable carboranes for uranium capture and release. *Nature* **2020,** 577, 652-+.

11. Dam, H. H.; Reinhoudt, D. N.; Verboom, W. Multicoordinate ligands for actinide/lanthanide separations. *Chem. Soc. Rev.* **2007,** 36, 367-377.

12. Ansari, S. A.; Pathak, P.; Mohapatra, P. K.; Manchanda, V. K. Chemistry of Diglycolamides: Promising Extractants for Actinide Partitioning. *Chem. Rev.* **2012,** 112, 1751-1772.

13. Pasquale, S.; Sattin, S.; Escudero-Adan, E. C.; Martinez-Belmonte, M.; de Mendoza, J. Giant regular polyhedra from calixarene carboxylates and uranyl. *Nature Commun.* **2012,** 3, 785.

14. Lee, J.; Brewster, J. T.; Song, B.; Lynch, V. M.; Hwang, I. H.; Li, X. P.; Sessler, J. L. Uranyl dication mediated photoswitching of a calix[4]pyrrole-based metal coordination cage. *Chem. Commun.* **2018,** 54, 9422-9425.

15. Kravchuk, D. V.; Forbes, T. Z. In Situ Generation of Organic Peroxide to Create a Nanotubular Uranyl Peroxide Phosphate. *Angew. Chem. Int. Ed.* **2019,** 58, 18429-18433.

16. Qiu, J.; Burns, P. C. Clusters of Actinides with Oxide, Peroxide, or Hydroxide Bridges. *Chem. Rev.* **2013,** 113, 1097-1120.

17. Gilson, S. E.; Li, P.; Szymanowski, J. E. S.; White, J.; Ray, D.; Gagliardi, L.; Farha, O. K.; Burns, P. C. In Situ Formation of Unprecedented Neptunium-Oxide Wheel Clusters Stabilized in a Metal-Organic Framework. *J. Am. Chem. Soc.* **2019,** 141, 11842-11846.

18. Dembowski, M.; Olds, T. A.; Pellegrini, K. L.; Hoffmann, C.; Wang, X. P.; Hickam, S.; He, J. H.; Oliver, A. G.; Burns, P. C. Solution P-31 NMR Study of the Acid-Catalyzed Formation of a Highly Charged {U(24)Pp(12)} Nanocluster, [(UO2)(24)(O-2)(24)(P2O7)(12)](48-), and Its Structural Characterization in the Solid State Using Single-Crystal Neutron Diffraction. *J. Am. Chem. Soc.* **2016,** 138, 8547-8553.

19. Soderholm, L.; Almond, P. M.; Skanthakumar, S.; Wilson, R. E.; Burns, P. C. The structure of the plutonium oxide nanocluster [Pu38O56Cl54(H2O)(8)](14-). *Angew. Chem. Int. Ed.* **2008,** 47, 298-302.

20. Fasting, C.; Schalley, C. A.; Weber, M.; Seitz, O.; Hecht, S.; Koksch, B.; Dernedde, J.; Graf, C.; Knapp, E. W.; Haag, R.

Multivalency as a Chemical Organization and Action Principle. *Angew. Chem. Int. Ed.* **2012,** 51, 10472-10498.

21. Badjic, J. D.; Nelson, A.; Cantrill, S. J.; Turnbull, W. B.; Stoddart, J. F. Multivalency and cooperativity in supramolecular chemistry. *Acc. Chem. Res.* **2005,** 38, 723-732.

22. Ercolani, G. Assessment of cooperativity in self-assembly. *J. Am. Chem. Soc.* **2003,** 125, 16097-16103.

23. Li, X. Z.; Zhou, L. P.; Yan, L. L.; Dong, Y. M.; Bai, Z. L.; Sun, X. Q.; Juan, D. W.; Shuao, W.; Bunzli, J. C.; Sun, Q. F. A supramolecular lanthanide separation approach based on multivalent cooperative enhancement of metal ion selectivity. *Nature Commun.* **2018,** 9, 547.

24. Wagle, D. V.; Kelley, S. P.; Baker, G. A.; Sikligar, K.; Atwood, J. L. An Indium-Seamed Hexameric Metal-Organic Cage as an Example of a Hexameric Pyrogallol[4]arene Capsule Conjoined Exclusively by Trivalent Metal Ions. *Angew. Chem. Int. Ed.* **2020,** 59, 8062-8065.

25. Hu, X. Q.; Chai, J.; Zhang, C.; Lang, J. X.; Kelley, S. P.; Feng, S. S.; Liu, B.; Atwood, D. A.; Atwood, J. L. Biomimetic Self-Assembly of Co-II-Seamed Hexameric Metal-Organic Nanocapsules. *J. Am. Chem. Soc.* **2019,** 141, 9151-9154.

26. Rathnayake, A. S.; Fraser, H. W. L.; Brechin, E. K.; Dalgarno, S. J.; Baurneister, J. E.; Rungthanaphatsophon, P.; Walensky, J. R.; Barnes, C. L.; Atwood, J. L. Oxidation State Distributions Provide Insight into Parameters Directing the Assembly of Metal-Organic Nanocapsules. *J. Am. Chem. Soc.* **2018,** 140, 13022-13027.

27. Rathnayake, A. S.; Fraser, H. W. L.; Brechin, E. K.; Dalgarno, S. J.; Baumeister, J. E.; White, J.; Rungthanaphatsophon, P.; Walensky, J. R.; Barnes, C. L.; Teat, S. J.; Atwood, J. L. In situ redox reactions facilitate the assembly of a mixed-valence metal-organic nanocapsule. *Nature Commun.* **2018,** 9, 2119.

28. Su, K. Z.; Wu, M. Y.; Yuan, D. Q.; Hong, M. C. Interconvertible vanadium-seamed hexameric pyrogallol[4]arene nanocapsules. *Nature Commun.* **2018,** 9, 4941.

29. Su, K. Z.; Wu, M. Y.; Wang, W. J.; Zhou, M.; Yuan, D. Q.; Hong, M. C. 3D metal-organic frameworks based on lanthanide-seamed dimeric pyrogallol[4]arene nanocapsules. *Science China-Chemistry* **2018,** 61, 664-669.

30. Zhang, C.; Patil, R. S.; Liu, C.; Barnes, C. L.; Atwood, J. L. Controlled 2D Assembly of Nickel-Seamed Hexameric Pyrogallol[4]arene Nanocapsules. *J. Am. Chem. Soc.* **2017,** 139, 2920-2923.

31. Kumari, H.; Deakyne, C. A.; Atwood, J. L. Solution Structures of Nanoassemblies Based on Pyrogallol[4]arenes. *Acc. Chem. Res.* **2014,** 47, 3080-3088.

32. Kumari, H.; Mossine, A. V.; Kline, S. R.; Dennis, C. L.; Fowler, D. A.; Teat, S. J.; Barnes, C. L.; Deakyne, C. A.; Atwood, J. L. Controlling the Self-Assembly of Metal-Seamed Organic Nanocapsules. *Angew. Chem. Int. Ed.* **2012,** 51, 1452-1454.

33. Abrahams, B. F.; Fitzgerald, N. J.; Robson, R. Cages with Tetrahedron-Like Topology Formed from the Combination of Cyclotricatechylene Ligands with Metal Cations. *Angew. Chem. Int. Ed.* **2010,** 49, 2896-2899.

34. McKinlay, R. M.; Cave, G. W. V.; Atwood, J. L. Supramolecular blueprint approach to metal-coordinated capsules. *P. Natl. Acad. Sci. USA* **2005,** 102, 5944-5948.

35. Luo, W.; Xiao, G.; Tian, F.; Richardson, J. J.; Wang, Y. P.; Zhou, J. F.; Guo, J. L.; Liao, X. P.; Shi, B. Engineering robust metal-phenolic network membranes for uranium extraction from seawater. *Energ Environ Sci* **2019,** 12, 607-614.

36. Li, B.; Ma, L. J.; Tian, Y.; Yang, X. D.; Li, J.; Bai, C. Y.; Yang, X. Y.; Zhang, S.; Li, S. J.; Jin, Y. D. A catechol-like phenolic ligand-functionalized hydrothermal carbon: One-pot synthesis, characterization and sorption behavior toward uranium. *J. Hazard. Mater.* **2014,** 271, 41-49.

37. Redmond, M. P.; Cornet, S. M.; Woodall, S. D.; Whittaker, D.; Collison, D.; Helliwell, M.; Natrajan, L. S. Probing the local coordination environment and nuclearity of uranyl(VI) complexes in non-aqueous media by emission spectroscopy. *Dalton Trans.* **2011,** 40, 3914-3926.

38. Surbella, R. G.; Ducati, L. C.; Autschbach, J.; Deifel, N. P.; Cahill, C. L. Thermochromic Uranyl Isothiocyanates: Influencing Charge Transfer Bands with Supramolecular Structure. *Inorg. Chem.* **2018,** 57, 2455-2471.

39. Shao, L.; Hua, B.; Hu, X. Q.; Stalla, D.; Kelley, S. P.; Atwood, J. L. Construction of Polymeric Metal-Organic Nanocapsule Networks via Supramolecular Coordination-Driven Self-Assembly. *J. Am. Chem. Soc.* **2020,** 142, 7270-7275.

40. Xie, Y. C.; Zhang, C.; Hu, X. Q.; Zhang, C.; Kelley, S. P.; Atwood, J. L.; Lin, J. Machine Learning Assisted Synthesis of Metal-Organic Nanocapsules. *J. Am. Chem. Soc.* **2020,** 142, 1475-1481.

41. Neal, H. A.; Szymanowski, J.; Fein, J. B.; Burns, P. C.; Nyman, M. Benchmarking Uranyl Peroxide Capsule Chemistry in Organic Media. *Eur. J. Inorg. Chem.* **2017**, 39-46.

SYNOPSIS TOC